Ion energy distribution and gas heating in the cathode fall of a direct-current microdischarge

Tsuyohito Ito* and Mark A. Cappelli
Mechanical Engineering Department, Stanford University, Stanford, California 94305-3032, USA
(Received 19 December 2005; published 14 April 2006)

This paper reports on measurements of the ion energy distribution (IED) at the cathode of an argon dc microdischarge using energy-resolved molecular beam mass spectrometry. The measurements are conducted at a fixed pressure-electrode separation product (pd) of 1 cm Torr with a maximum discharge pressure of 20 Torr. The measured IED is compared to the theory of Davis and Vanderslice [W. D. Davis and T. A. Vanderslice, Phys. Rev. **131**, 219 (1963)]. A higher pressure in a case of almost constant normalized current densities by pressure ($Jp^{-2}=0.080\pm0.006$ mA/cm^{-2} Torr^{-2}) yields a lower ratio of the ion mean free path to the sheath thickness. The results in almost constant Jp^{-2} case then indicate that a scaling law of Jp^{-2} is no longer applicable for IED of microdischarge. Expected background gaseous temperatures from IEDs with the collisional Child law have reasonable increasing with increased current density (J) in both cases of almost constant Jp^{-2} and a constant pressure of 10 Torr. Supported by temperature measurement by laser absorption spectroscopy, it is demonstrated that the expanded theory might be applicable also to microdischarges (Ar$\sim$20 Torr) with temperature adjusting.

DOI: 10.1103/PhysRevE.73.046401 PACS number(s): 52.80.−s, 82.20.Rp, 52.40.Hf

I. INTRODUCTION

In dc glow discharges, the cathode sheath is responsible for the creation of energetic ions, which, upon striking the cathode surface, create secondary electrons necessary for sustaining the discharge. These secondary electrons are accelerated by the cathode fall to an energy sufficient for direct collisional ionization. In some glow discharge applications, the ions bombarding the cathode are used in surface treatment, etching, sputtering, and ion-assisted deposition. A dc microdischarge, characterized by electrode separations of order 1 mm or less, has a relatively high cathode surface area to volume ratio. Furthermore, extending the size of discharges to the microscale requires operation at relatively high pressures (10–100 Torr) in order to preserve the pressure—electrode separation (pd) product, a result of the usual scaling of gas discharges [1,2] when gas heating is neglected. A departure from this usual scaling law must be considered for a microdischarge. Since, in a parallel electrode configuration, the heat conducted to the electrodes scales inversely with the electrode separation, d, whereas the Ohmic heat generated scales inversely with d^2, then a consequence of a reduced separation to preserve a pd scaling results in an elevation in the gas temperature. Gas heating is not commonly considered in the modeling of the cathode fall of lower pressure glow discharges. Understanding the cathode fall (sheath) and its associated physical phenomena including ion transport, the development of the ion energy distribution, and the heating of the neutrals in microdischarges is critical to the understanding of the applications of these devices to the development of novel light sources [3], processing plasmas [4], micropropulsion devices [5], among others.

Some of the earliest experimental and theoretical work on the ion energy distribution (IED) in dc discharges was performed by Davis and Vanderslice [6] in the early 1960s. In that study, they show that the structure of the IED should depend largely on the ratio of the ion mean free path, λ_i, to the sheath thickness, S. This scaling has been supported by numerous subsequent studies [7–12], in some cases to values of the electric field to neutral number density ratio, E/n as high as 2×10^{-7} V m^2 in Ar [8]. Included in these studies are direct measurements of the IED at the cathode although the pressures considered have been no higher than a few Torr. In almost all cases [6–9], an analysis of the results assumes that the elevation in the background gas temperature is negligible—a reasonable assumption for experiments carried out at pressures in the few Torr range or less, with electrodes of sufficient size capable of providing an adequate thermal reservoir. More recently, there have been some experimental and theoretical studies of the impact of thermal heating of the background gas in argon [12–15] and in helium [16] dc glow discharges. Measurements were also made by laser absorption of the elevated temperatures in argon dc microhollow cathode discharges [17]. The simulations of Revel *et al.* [13] confirm that the affect on the discharge associated with thermal heating is insignificant at typical current densities (<4 mA cm^{-2}) and pressures ($\leqslant1$ Torr) associated with low pressure dc glow discharges. However, at higher current densities and at even modest pressure levels (3 Torr), the temperature elevation becomes significant [14,15]. In atmospheric pressure microhollow cathode discharges, the temperatures recorded were nearly 2000 K [18]. Microdischarges, which often operate a relatively high pressure environment, have a concomitantly higher current density, and so it is expected that in comparison to conventional macroscale discharges, will operate at higher temperatures, as predicted by consideration of the scaling of the energy deposition and transport processes as discussed above.

In this paper, we report on measurements of the energy distribution of ions at the cathode of an argon planar dc microdischarge, with an electrode separation as low as d

*Email address: tsuyohito@stanford.edu

$=500\ \mu$m. The ion energy is characterized by energy-resolved mass spectrometry. The discharge pressure is varied to as high as $p=20$ Torr, with mass spectrometry and sampling through the cathode facilitated by differential pumping stages. We show that the theory of Davis and Vanderslice [6] with a sheath potential variation proposed by Budtz-Jørgensen *et al.* [9] leads to a reasonable description in the observed energy spectra at these higher pressures if we account for Ohmic heating of the background gas. Doppler-broadened spectral absorption measurements using a cw laser tuned to an excited state in neutral argon is used to confirm the relatively high gas temperature and its dependence on the discharge pressure and reduced current density. In addition to confirming the importance of thermal heating in these dc microdischarges, we quantify its affect on the interpretation of the applicability of simplified models for ion transport and ion energy distribution.

II. EXPERIMENT

A. Ion energy distribution measurements

The dc microdischarge used here is generated between planar electrodes comprised of a grounded stainless-steel (foil) cathode and a carbon steel anode in argon (Ar) at a pressure of $p=2-20$ Torr. Voltage is applied to the anode through a ballast resistance ($10\ k\Omega-1$ MΩ) and the discharge current is monitored at the anode side using an ammeter that is electrically floating at anode potential. The anode is mounted to a three-dimensional translation stage allowing adjustment of the electrode separation (d). In the study reported on here, the separation is varied between 500 and 5000 μm or the pressure is varied between 2 and 20 Torr while keeping pd constant at a value of $pd=1$ cm Torr. The cathode, which has a thickness of about 60 μm, is held at ground potential. The cathode surface is masked by alumina (mainly to prevent unwanted discharging from the cathode edge), defining an exposed cathode diameter of 6.3 mm. The positive discharge voltage applied to the anode is corrected for the voltage drop across the ballast resistance. The current density (J) is determined from the measured current and exposed cathode area, assuming a uniform current distribution. Qualitative visual (and photographic confirmation) is made of the discharge to ensure that the plasma uniformly fills the space between the electrodes, and operates in the abnormal glow regime. Figure 1 presents a compilation of the discharge current density and voltage for all operating points at which ion energy distributions are measured in this study. It is noted that the current density is scaled by pressure (Jp^{-2}) in accordance with the usual scaling laws as presented by Phelps [19]. As discussed by Phelps [19], the appropriate scaling parameters for abnormal glow discharges are Jn^{-2}, nd, and E/n, where n is the neutral number density. The conventional use of pressure (p) in place of n is due to the usual assumption that the gas temperature is uniform and close to room temperature. The measurements in Fig. 1 appear to collapse onto a curve over the range of pressure investigated, with the measured discharge voltage generally increasing with the scaled current density

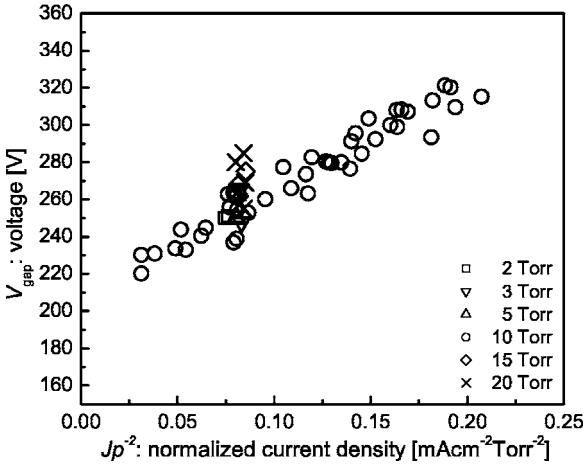

FIG. 1. Discharge voltage variation with normalized current density (Jp^{-2}).

Jp^{-2}, as expected for an abnormal glow discharge. The experimental scatter for the 10 Torr data is partly due to irregularities in the electrode surface [8]. In the course of this study, we periodically polished the electrode surface to maintain reasonable reproducibility in the discharge current and voltage.

A schematic diagram of the experimental arrangement used for measuring the IED is given in Fig. 2. In order to successfully sample ions from the microdischarge, which is operated at a relatively high pressure, the microdischarge is attached to a chamber equipped with differential pumping stages. Ions incident on the cathode in the discharge stage (2–20 Torr) pass through a 20 μm diameter pinhole. The ions subsequently drift through this intermediate stage ($<10^{-4}$ Torr), and enter the independently pumped mass spectrometer (Hiden model No. EQP-300). The mass spectrometer is equipped with a sector-field energy analyzer and quadrupole mass filter. This facility allows us to discriminate between the positive charge carriers in a gas mixture, although only pure argon discharges are reported on here. Even at the highest voltages studied ($\sim$320 V) the measured IED is well within 100 eV, which is the maximum energy limit of the analyzer. With the discharge at a pressure of

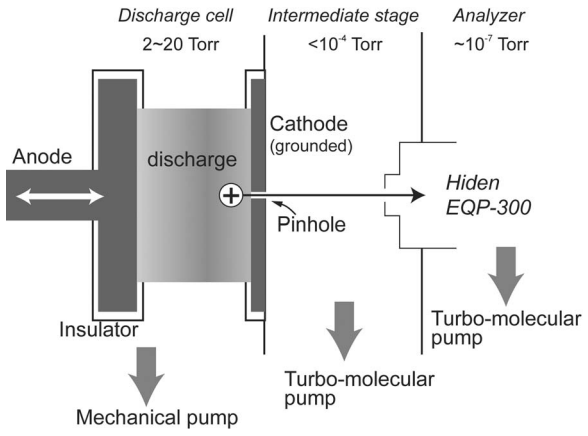

FIG. 2. Experimental schematic for ion energy distribution measurements.

20 Torr, the analyzer stage is maintained at a pressure of approximately 10^{-7} Torr.

We performed two series of experiments at a fixed value of $pd=1$ cm Torr. In the first series, the pressure was varied while maintaining a constant normalized current density $Jp^{-2}=0.080\pm0.006$ mA cm^{-2} Torr^{-2}. The second series of experiments was carried out by changing the normalized current density over the range $Jp^{-2}=0.03-0.21$ mA cm^{-2} Torr^{-2} while at a fixed pressure of $p=10$ Torr ($d=1$ mm). These experiments serve to test the Jp^{-2} scaling of the discharge voltage (see Fig. 1) and the validity of the theory of Davis and Vanderslice [6] for ion energy distributions under microdischarge conditions at pressures up to 20 Torr. Both sets of experiments allowed us to examine the affect of gas heating, if any, which has been largely ignored in most glow discharge studies.

In interpreting the measured IED, $f(\tilde{\varepsilon}_i)$, we use the theory of Davis and Vanderslice [6], modified by Budtz-Jørgensen *et al.* [9] to account for a sheath potential variation that is in better agreement with particle-in-cell simulations. The resulting distribution (expressed in terms of the normalized ion energy $\tilde{\varepsilon}_i=\varepsilon_i/eV_d$) is given here as

$$f(\tilde{\varepsilon}_i)=\frac{3}{5}\frac{S}{\lambda_i}(1-\tilde{\varepsilon}_i)^{-2/5}\exp\left\{-\frac{S}{\lambda_i}[1-(1-\tilde{\varepsilon}_i)^{3/5}]\right\}. \quad (1)$$

In deriving the IED, it is assumed that (i) there is negligible ionization within the cathode fall, (ii) ions lose all their energy in a collision, and (iii) the ion collision cross section, σ_{cx}, is independent of ion energy. Assumption (ii) is supported by the dominance of the resonance charge transfer collision process between Ar and Ar^+ for the range of E/n expected in our experiments [8]. This resonant charge exchange cross section is believed to vary between approximately 6×10^{-19} m^2 and 4×10^{-19} m^2, over a range of energy of 1–100 eV, respectively [20]. A value of 5×10^{-19} m^2 is employed in this study, consistent with the value extracted from experiments by Davis and Vanderslice [6]. One can find reference to a range of values for this cross section derived from experiments, e.g., $3.7-5.3\times10^{-19}$ m^2 in dc glow discharges [6,9] and $4-7.2\times10^{-19}$ m^2 in uniform electric field experiments [8]. Equation (1) indicates that the IED depends exclusively on the ratio of the sheath thickness to the ion mean free path. This ratio also enters into the collisional form of the Child-Langmuir Law for the current density variation with discharge voltage, expressed here as [9]

$$J=\left(\frac{2}{3}\right)\left(\frac{5}{3}\right)^{3/2}\varepsilon_0\left(\frac{2e}{\pi M}\right)^{1/2}\left(\frac{\sigma_{cx}}{kT_g}\right)^2\frac{V_d^{3/2}p^2}{(S/\lambda_i)^{5/2}}. \quad (2)$$

Here, ε_0 is the free space permittivity, and T_g is the gas temperature, which is assumed to be constant within the cathode sheath. In previous measurements of the IED in low pressure (<1 Torr) argon discharges [9], the ratios S/λ_i determined from the measured distributions [according to Eq. (1)] were used along with the measured J, p, and V_d, and with the collisional Child-Langmuir law to determine σ_{cx} under the assumption that there is little or no gas heating. In our studies described below, carried out at higher pressure, we demonstrate conclusively that while such as assumption is valid at pressures below a few Torr, it cannot be applied at the highest pressures investigated by us (~20 Torr), where we find that the temperature elevation can exceed 700 K. A further complication can arise in applying these theories to high pressure, when there is a strong variation in the gas temperature (number density) within the sheath itself. While our temperature measurements described in the next section cannot resolve these possible nonuniformities, we carry out a simple analysis in the Appendix that suggests that over the pressure range investigated, the discharge cannot support strong thermal gradients at our dissipated power levels. In our conditions, the temperature nonuniformities that may exist give rise to only minor departures in the IED from those predicted by the simple theory of Davis and Vanderslice [6], certainly well within the accuracy of our experiments. However, at higher pressures, strong thermal gradients over scales comparable to the sheath thickness would require a reexamination of the theory.

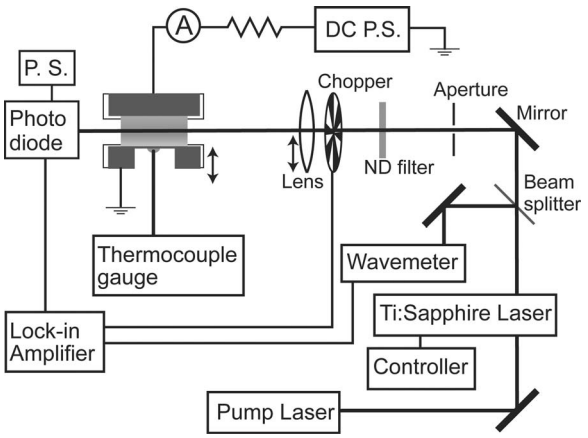

FIG. 3. Experimental schematic laser absorption measurements.

B. Temperature measurements by laser absorption spectroscopy

Figure 3 depicts a schematic diagram of the implementation of laser absorption spectroscopy (LAS) used for characterizing the discharge gas temperature. In these measurements, the position of the cathode is varied relative to the fixed anode. A thermocouple attached to the backside of the thin cathode is used to estimate the cathode temperature. The tunable, narrow-band (1–10 MHz bandwidth) output from a Ti:sapphire laser (Coherent, model No. 899-21) pumped by a diode-pumped Nd:yttrium-aluminum-garnet (YAG) laser (Coherent, model Verde) is focused using a 40 cm focal length lens into the center of the discharge along a direction parallel to the electrodes and used to probe absorption of the 811.5 nm ($1s_5$-$2p_9$) excited electronic transition in argon, originating on the metastable ($1s_5$) electronic state. The laser is chopped to facilitate detection of the transmitted beam recorded on a photodiode using a lock-in amplifier (Stanford Research Systems model No. SR850). A portion of the laser probe beam is split from the main beam and directed into a

wavemeter (Burleigh model No. WA-1000) for monitoring of the laser wavelength. The probe laser wavelength is scanned across the 811.5 nm spectral line at a rate of 20 GHz/min. The focused beam waste, aligned to coincide with the center of the discharge, is estimated to be 250–300 μm. This beam waist, which is comparable in size to the separation between the electrodes in some cases, precluded an accurate measure of the spatial distribution in the gas temperature, at this time. Although the species probed by laser absorption is in an electronically excited state of argon, it is assumed that this excited state is populated primarily by excitation of the ground state by electron collisions, and that the Doppler-shifted absorption spectrum represents the distribution of ground-state velocity component in a plane normal to the discharge axis. Previous studies of emission in argon glow discharges confirm that the temperature of electronically excited argon atoms is equal to that of the background argon [21]. Penache *et al.* [17] and Tachibana *et al.* [22] also employed similar laser absorption measurements on an excited electronic state for Doppler characterization of the gas temperature in an argon glow discharge. It is noteworthy that while the laser beam may partially probe a region overlapping with the cathode fall, and the neutral argon component in the cathode fall can gain energy along a direction parallel to the discharge axis due to charge exchange with energetic ions, the motion in a plane normal to the axis will preserve the random (thermal) component of the velocity distribution and the absorption spectrum should therefore characterize the gas temperature.

For the analysis of the LAS spectra, we assume that the discharge is uniform along a direction coinciding with the path of the probe laser. The transmitted laser intensity (I) will be attenuated when compared to the incident intensity (I_0) in accordance with the Beer-Lampert law

$$I = I_0 \exp[-k(\nu)\ell]. \tag{3}$$

Here, $k(\nu)$ is the frequency-dependent absorption coefficient, which is proportional to the spectral lineshape, and ℓ is the absorption path length (equal in this case to the discharge diameter). The measured spectral line shape, proportional to $\ln(I/I_o)$, will have a Voigt shape characteristic of a convolution between a Gaussian component (due to Doppler broadening) and a Lorentzian component (primarily due to collisional broadening). The full width at half maximum (FWHM), $\Delta\nu_D$ of the Doppler broadened component is given here as

$$\Delta\nu_D = \frac{2\nu_0}{c}\sqrt{\frac{2k_BT\ln 2}{M}}, \tag{4}$$

here ν_0 is spectral line center frequency, c is the light speed, k_B is the Boltzmann constant, M is the argon mass, and T is the temperature.

In our measurements, the Lorentzian width is found to comprise about 10% of the total spectral width. Experimental uncertainty associated with an accurate determination of the spectral absorption base line precluded use of this Lorentzian component measurement to accurately confirm the pressure-broadening constant for this transition. However, our results are found to be within the range determined by Tachibana *et al.* [22] for this electronic transition.

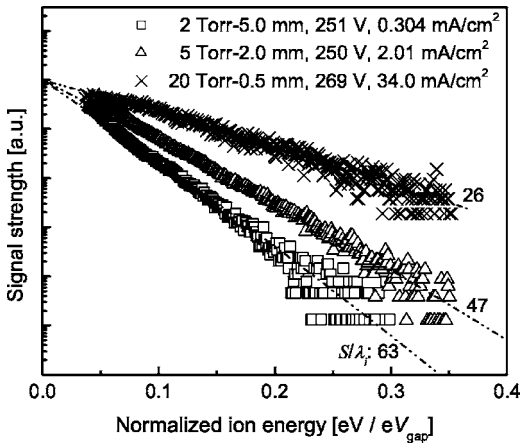

FIG. 4. Ar^+ energy distribution for normalized current densities (Jp^{-2}) of 0.080 ± 0.006 mA/cm^{-2} Torr^{-2} (pd=10 mm Torr).

III. RESULTS AND DISCUSSION

Examples of the observed cathode-incident Ar^+ energy distributions under conditions of pd=1 cm Torr and a reduced current density $Jp^{-2}=0.080\pm0.006$ mA cm^{-2} Torr^{-2} are shown in Fig. 4. It is noteworthy that only minor adjustments in voltage are needed to maintain a constant value for Jp^{-2}. According to the collisional Child-Langmuir law [Eq.(2)], the corresponding ratio S/λ_i should vary only slightly for the range of operating conditions studied. Application of Eq.(1) to an analysis of these energy distributions give the dashed lines that are superimposed onto the data in the figure. The ratio S/λ_i is adjusted in each case until an acceptable fit to the distributions is obtained. While the theory of Davis and Vanderslice captures the shape of the distributions reasonably well, it is apparent that the differences in the required S/λ_i values needed to obtain agreement to theory is significant, in contrast to that predicted by Eq.(2). As described below, we attribute this discrepancy to the effect of gas heating, predominantly at the higher operating pressures investigated.

The ratios S/λ_i extracted from the energy distributions for the complete range of conditions examined are presented as the open circles in Fig. 5. Also plotted as the open diamonds, are the corresponding values determined from the collisional Child-Langmuir law, assuming a temperature of 300 K. While good agreement between the two measurements is obtained at low pressure, the disparity increases with increasing pressure. The suspected parameter that could account for this increased disagreement is the gas temperature. In Fig. 6 we plot the adjustments in the gas temperature used in the collisional Child-Langmuir law that are necessary in order to bring these two sets of data into agreement. It is noteworthy that the estimated temperature depends on the value used for the charge exchange cross section. We see that the corresponding gas temperature must necessarily increase with increased pressure; an expected consequence associated with

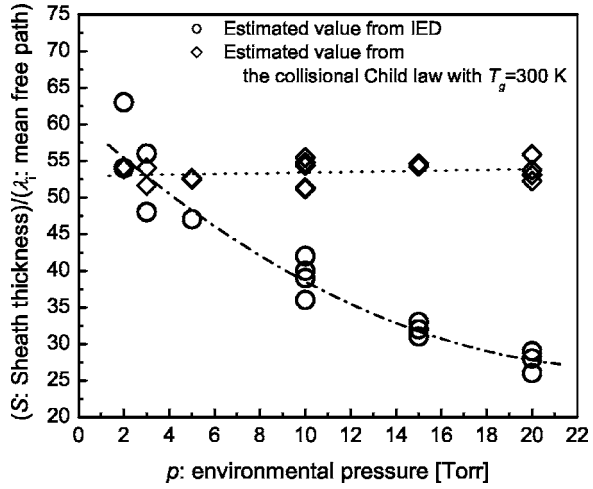

FIG. 5. Ratio of the sheath thickness to mean free path for normalized current densities (Jp^{-2}) of 0.080 ± 0.006 mA/cm^{-2} Torr^{-2}: circles—values extracted from the ion energy distributions (Fig. 4) and diamonds—from the collisional Child law with T_g=300 K.

the different scaling behavior associated with the Ohmic dissipation and heat flux as discussed above.

Figure 7 presents representative Ar^+ energy distributions at a pressure of 10 Torr, while varying the reduced current density over the range Jp^{-2}=0.03–0.21 mA/cm^{-2} Torr^{-2}. Again, superimposed onto these data are the theoretical curves of Eq. (1), with the ratios S/λ_i adjusted to obtain a reasonable fit to the measured distributions. The variations in the extracted ratios S/λ_i with Jp^{-2} for the entire data set are summarized as the open circles in Fig. 8. Also indicated in this figure are the ratios obtained from the collisional Child-Langmuir law assuming a gas temperature T_g=300 K (open diamonds). The values obtained from the measured energy distributions are consistently lower than those obtained from

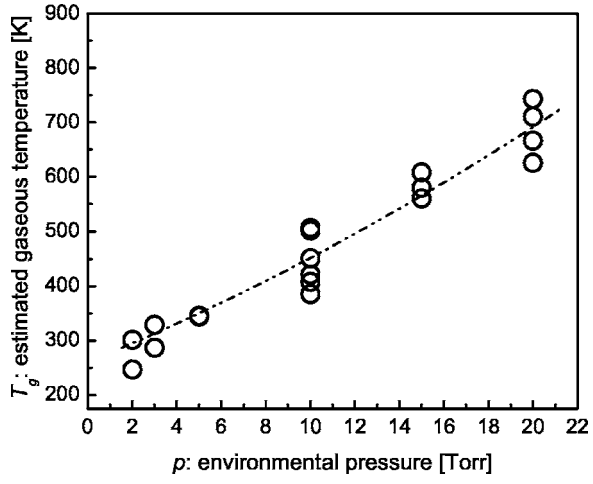

FIG. 6. Gas temperature required for agreement between the ratio of the sheath thickness to ion mean free path extracted from the ion energy distribution and from the collisional Child law. The conditions are for normalized current densities (Jp^{-2}) of 0.080 ± 0.006 mA/cm^{-2} Torr^{-2}. The dashed line represents a fit to the data.

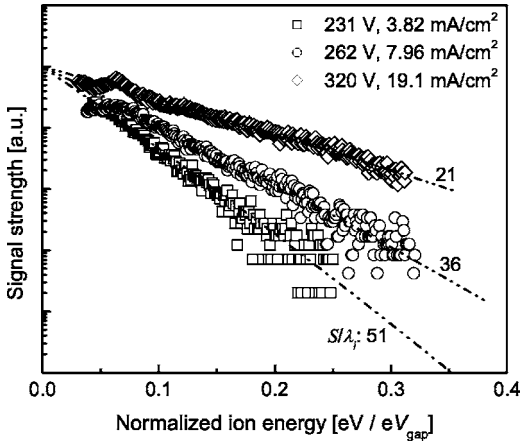

FIG. 7. Ar^+ energy distribution measured for 10 Torr–1 mm gap, while varying the normalized current density.

the Child-Langmuir law, with the differences increasing with increased current density. This difference can be accounted for by an increased gas temperature. In Fig. 9, we plot the temperature that would be required in order to bring these two data sets into agreement. Despite the scatter in this data, there is a clear upwards trend in the temperature with increased current density; also an expected consequence associated with increased Ohmic dissipation.

Laser absorption spectroscopy was used to confirm the expected increase in gas temperature with increasing pressure and current density. A representative lineshape obtained from a typical absorption scan of the 811.5 nm transition is shown in Fig. 10. Also shown is a Voigt function constructed from the convolution of a normalized Gaussian and Lorentzian line shape, with their corresponding FWHM adjusted to obtain good agreement with the measured profile. It is noteworthy that the optimization of the fit with two adjustable parameters is facilitated by the fact that the Lorentzian component mainly affects the spectral line wings, while the Gaussian (Doppler) component most strongly influences the

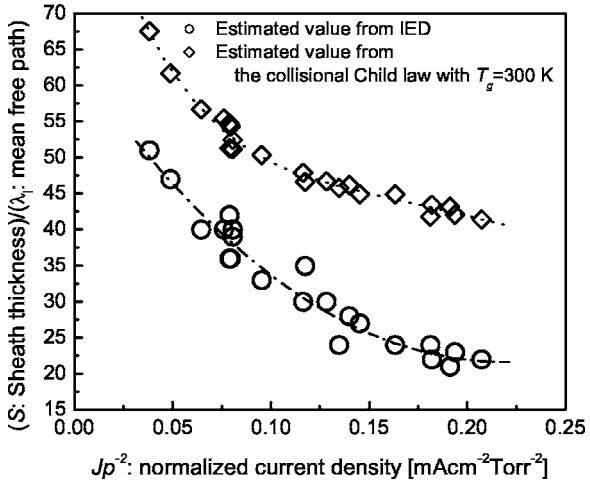

FIG. 8. Sheath thickness to mean free path ratio for 10 Torr–1 mm gap conditions: circles—values extracted from the ion energy distributions (Fig. 7); diamonds—from the collisional Child law with T_g=300 K.

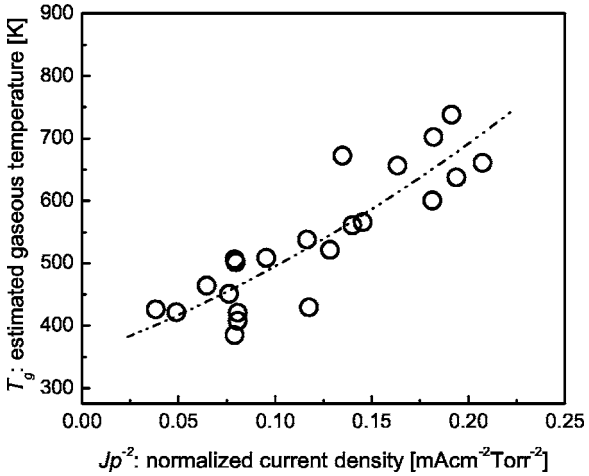

FIG. 9. Gas temperature required for agreement between the sheath thicknesses to mean free path ratio extracted from the ion energy distribution and from the collisional Child law for 10 Torr–1 mm gap conditions. The dashed line represents a fit to the data.

shape of the spectral line core. For this particular spectral lineshape, the "best fit" Doppler width is $\Delta\nu_D=0.98$ GHz, corresponding to a temperature of $T_g=543$ K. The "best fit" Lorentzian width is $\Delta\nu_D=0.09$ GHz, which is within the range expected for pressure broadening [22].

Figures 11 and 12 summarize the temperatures measured by LAS, for the cases where pressure and reduced current density are varied, respectively. Also illustrated in these figures is a line representing the trends seen in the temperatures obtained in Figs. 6 and 9. The agreement between these temperatures is remarkably good, certainly within experimental uncertainty, and reinforces our understanding of the effect that gas heating has on the scaling expected from the collisional Child-Langmuir law. It is noteworthy however, that the elevated temperatures measured by LAS are in the mid-gap region of the discharge, somewhat beyond the location of the sheath edge, and the temperatures are expected to fall

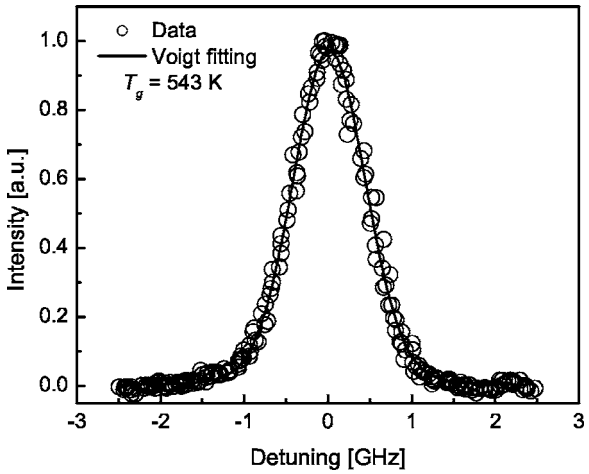

FIG. 10. Typical laser absorption spectrum and its associated Voigt fit for conditions of $p=10$ Torr, $d=1$ mm, and $Jp^{-2}=0.081$ mA/cm^{-2} Torr^{-2}.

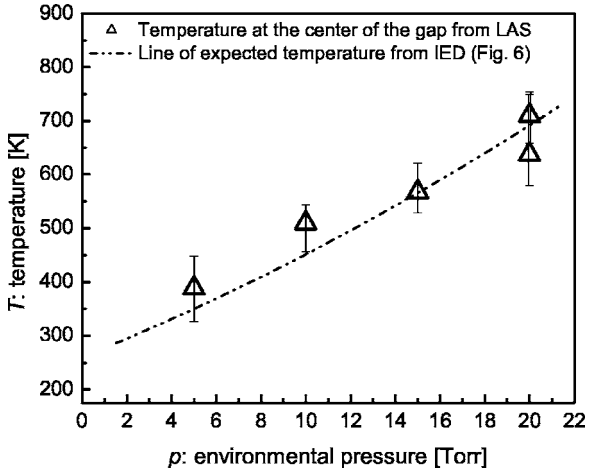

FIG. 11. A comparison of the temperature derived from LAS and the temperature fit to the data from Fig. 6 for normalized current densities (Jp^{-2}) of 0.080±0.006 mA/cm^{-2} Torr^{-2}.

slightly towards the electrodes in order to support the local heat flux. In the Appendix, we estimate that the temperature difference between the mid gap region and the cathode is no more than approximately 50 K if 25% of the discharge power is dissipated in the form of Ohmic heating [13]. A difference of 50 K is within the experimental uncertainty of our LAS temperature measurements. Thermocouple measurements were also made of the temperature on the backside of the thin cathode foil, the results of which are also plotted in Fig. 12. Despite our estimates of a 50 K temperature difference, there appears to be a relatively large temperature drop at the cathode surface (as much as 200 K). In the Appendix, we estimate that 100% of the discharge power would have to be invested into Ohmic heating to obtain such a temperature difference—an unlikely scenario. We believe that this difference instead can be accounted for by a temperature slip at the cathode surface, which is not uncommon in thermal transport at low gas density. The temperature slip (difference between the cathode temperature and adjacent gas temperature, ΔT_{cath}) is given by [23]

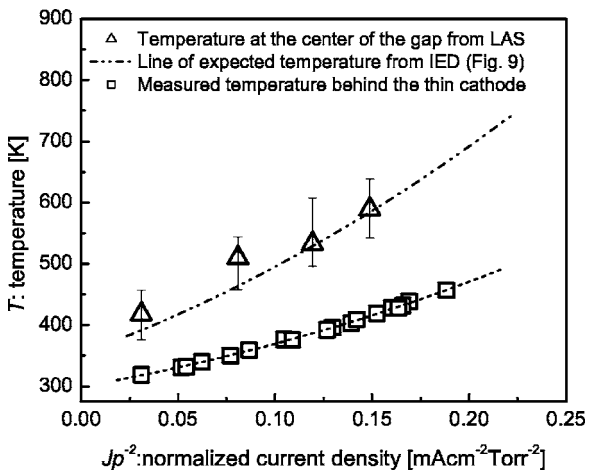

FIG. 12. A comparison of the temperature derived from LAS to the temperature fit from Fig. 9. Also shown is the temperature measured on the backside of the thin cathode for 10 Torr.

$$\Delta T_{cath} = \left(\frac{2-\alpha}{2\alpha}\right)\frac{\kappa_T}{pc_p}\left(\frac{2\pi k_B T_{g,cath}}{M}\right)^{1/2} \left.\frac{dT_g}{dx}\right|_{cath}, \quad (5)$$

$$= \left(\frac{2-\alpha}{2\alpha}\right)\frac{q}{pc_p}\left(\frac{2\pi k_B T_{g,cath}}{M}\right)^{1/2}. \quad (6)$$

Here κ_T is the thermal conductivity of the gas [24,25] which will depend on the gas temperature, and c_p is the specific heat capacity, taken to be approximately 523 $\mathrm{J/kg^{-1}\,K^{-1}}$ [26], M is the molecular mass of argon, and α is the energy accommodation coefficient. The heat flux, q, to the cathode is established by the gas temperature gradient, $q = \kappa_T \frac{dT_g}{dx}|_{cath}$. The maximum temperature slip (maximum gradient) is when $q = IV_d/2A$, i.e., when all of the discharge power is deposited into the background gas. Examining Eq. (6) for the 10 Torr discharge case where the current density $J = 15$ mA cm^{-2} (0.15 mA/cm^{-2} Torr^{-2}), we find that a temperature slip of $\Delta T_{cath} = 90$ K is possible if the temperature of the gas at the cathode surface is 590 K, and if we assume a reasonable value of $\alpha = 0.25$. This temperature slip would result in a cathode surface temperature of about 500 K, which is comparable to that measured (~420 K).

IV. CONCLUSIONS

Measurements were reported of the ion energy distribution of cathode-impinging ions in an Ar dc microdischarge. Experiments were carried out at $pd = 1$ cm Torr to a pressure as high as 20 Torr under conditions of constant Jp^{-2} (0.080 ± 0.006 mA/cm^{-2} Torr^{-2}) and at a pressure of 10 Torr with varying Jp^{-2} (0.03–0.21 mA/cm^{-2} Torr^{-2}). A comparison of the measured distributions to the theory of Davis and Vanderslice [6] allows an estimate of S/λ_i, which is in good agreement with that expected from the collisional form of Child's law at low pressure, or at low current density, where heating of the background neutral gases is expected to be negligible. However, a significant disagreement is seen at higher values of p, J, attributable to Ohmic heating. The difference can be accounted for by an increase in the background argon temperature. This increased temperature is verified by laser absorption spectroscopy. At the highest pressure and current density range examined, the argon temperature reaches values as high as approximately 700 K. The results provide convincing support for the applicability of the theory of Davis and Vanderslice, and for the collisional form of Child's law to microdischarges operating as high as 20 Torr. The results also demonstrate that under conditions where gas heating may be important, the proper scaling of the discharge voltage is Jn^{-2}, and not Jp^{-2}.

ACKNOWLEDGMENTS

The authors would like to thank W. S. Crawford and D. Scharfe for help with the experiments and for many useful suggestions. This research was supported by the Department of Energy under Grant No. DE-FG03-97ER54447-A005. Partial support for T. Ito was provided by JSPS.

APPENDIX

The theory of Davis and Vanderslice [6] for the ion energy distribution can be expanded to account for nonuniform temperature (density) variation in the cathode fall. We begin with Poisson's equation for the ion-rich sheath under conditions where the ion drift velocity is greater than the ion thermal velocity [27]

$$\frac{dE}{dx} = \frac{en_s u_s}{\varepsilon_0 (2e\lambda_i E/\pi M)^{1/2}} = \frac{J}{\varepsilon_0 (2ekT_g E/\pi M p \sigma_{cx})}. \quad (A1)$$

Here x is the distance from the cathode, e is the ion charge, n_s and u_s are the ion density and an ion velocity at the sheath edge respectively, ε_0 is the permittivity of free space, λ_i is the ion mean free path (for charge transfer), M is the ion mass, J is the ion current density (specified and constant), k is Boltzmann's constant, T_g is the neutral gas temperature (depends on x), p is the pressure (specified and constant), and σ_{cx} is the charge transfer cross section.

The gas temperature in the vicinity of the sheath is assumed to be a balance between heat conduction and Ohmic heating

$$\frac{d}{dx}\left(\kappa_T \frac{dT_g}{dx}\right) + \beta JE = 0. \quad (A2)$$

The factor β is a parameter (unknown) that characterizes the fraction of the total discharge power that results in Ohmic dissipation. Solution of Eqs. (A1) and (A2) require boundary conditions on T_g and E. The temperature and the sheath voltage are specified at the sheath edge, and their derivatives at the sheath edge are taken to be zero. Equations (A1) and (A2) are solved numerically by marching towards the cathode surface from the sheath edge. The cathode surface is determined to be where the plasma potential becomes 0 V—the defining condition for the sheath thickness. The plasma potential variation, $\varphi(x)$, in the sheath is obtained from integrating the electric field. This procedure is repeated by changing the specified gas temperature (at the sheath edge) until the desired gas temperature at the cathode surface is obtained (shooting method). The resulting calculation provides us with $T_g(x)$, and a measure of the difference, ΔT_g, between the gas temperature at the sheath edge, and that at the cathode surface.

Knowledge of the temperature variation in the sheath allows us to determine the number of ions, dN, that undergo charge transfer in the region dx at a position x and that subsequently strike the cathode without further collisions

$$dN = N_0 \frac{p\sigma_{cx}}{kT_g} \exp\left(-\int_0^x \frac{p\sigma_{cx}}{kT_g} dx'\right) dx. \quad (A3)$$

The cathode impinging ion energy distribution, $F(\varphi)$ is defined by

$$F(\varphi) = \left(\frac{dN}{dx}\frac{dx}{d\varphi}\right)_{x=x_\varphi} \quad (A4)$$

where x_φ is the inverted dependence of the position x on the local plasma potential φ, easily evaluated from $\varphi(x)$.

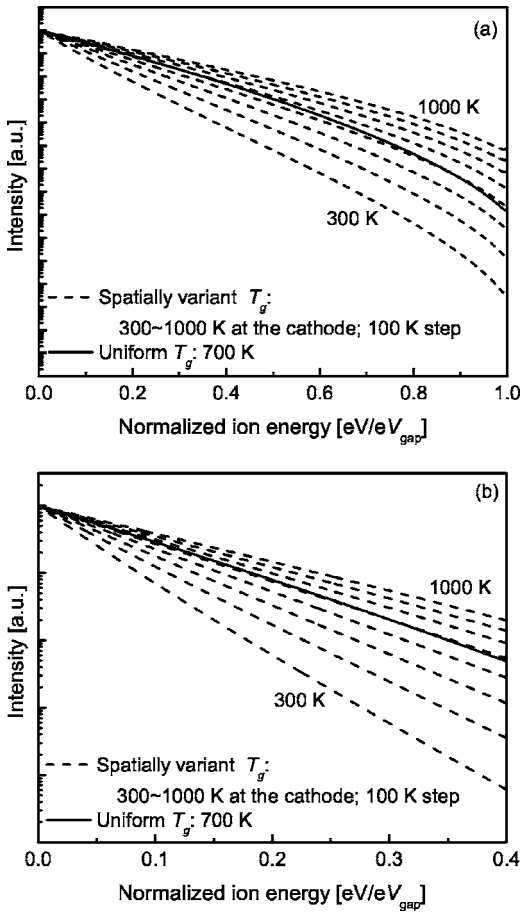

FIG. 13. Simulated ion energy distribution for conditions of $p=10$ Torr, $Jp^{-2}=0.207$ mA/cm^{-2} Torr^{-2}, and $V_0=315$ V: the spatially variant temperature model (300–1000 K at the cathode, based on the 100% Ohmic heating) and the uniform temperature model (700 K): (a) full ion energy range and (b) expanded range to cover range of energies measured in this study.

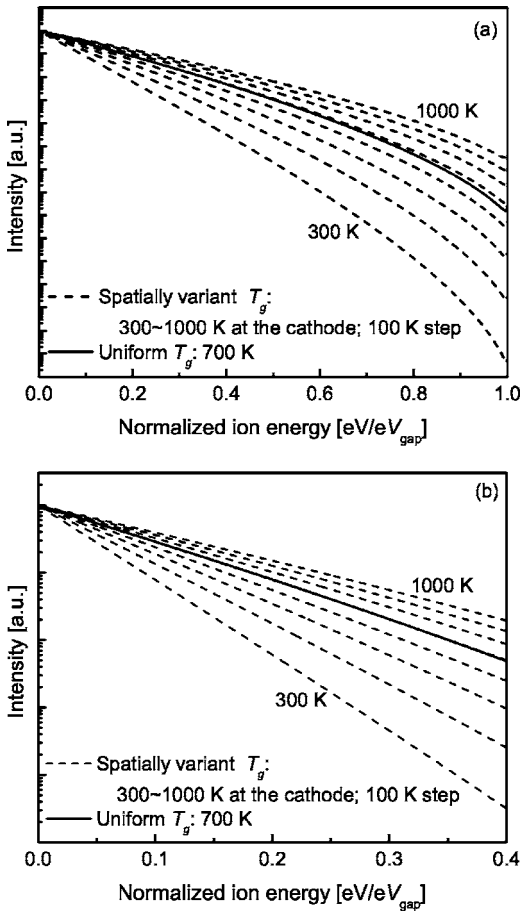

FIG. 14. Simulated ion energy distribution for conditions of $p=10$ Torr, $Jp^{-2}=0.207$ mA/cm^{-2} Torr^{-2}, and $V_0=315$ V: the spatially variant temperature model (300–1000 K at the cathode, based on the 25% Ohmic heating) and the uniform temperature model (700 K): (a) full ion energy range and (b) expanded range to cover range of energies measured in this study.

Computed ion energy distributions $F(\varphi)$ are presented in Figs. 13 and 14 for a range of values for the gas temperature at the cathode surface. In both figures, (b) is an expanded scale of (a), to cover the range of ion energy resolved in our experiments. The discharge conditions in Figs. 13 and 14 correspond to: $p=10$ Torr, $Jp^{-2}=0.207$ mA·cm^{-2} Torr^{-2}, and $V_0=315$ V—conditions where we expected large gas temperature differences between the sheath edge and the cathode surface. Figures 13 and 14 differ in the assumed fraction, β, of the discharge power that is channeled into gas heating. In Fig. 13, we assume that all of the discharge power is channeled into Ohmic heating, i.e., $\beta=1$. In Fig. 13, we take $\beta=0.25$. For comparison, in both figures, we also show the resulting IED for a uniform temperature $T_g=700$ K ($\beta=0$). In both cases, it is also apparent that differences between the ion energy distributions for the case of a uniform temperature (here, 700 K), and that of a nonuniform temperature in the sheath, appear only at large energies, i.e., $\tilde{\varepsilon}_i=\varepsilon_i/eV_d \geqslant 0.4$, above the energy range investigated in our experiments ($\tilde{\varepsilon}_i=\varepsilon_i/eV_d \leqslant 0.35$).

Although not shown, in Fig. 13, with $\beta=1$ the computed temperature difference ΔT_g varies from approximately $\Delta T_g=170$ K for $T_{g,cath}=1000$ K to $\Delta T_g=260$ K for $T_{g,cath}=300$ K. This should be contrasted with $\Delta T_g=45$ K for $T_{g,cath}=1000$ K to $\Delta T_g=80$ K for $T_{g,cath}=300$ K, when $\beta=0.25$, as in Fig. 14. This confirms that if heat conduction through the sheath were responsible for the observed differences between the measured temperatures near the discharge center, and the cathode temperature (of about 200 K at these conditions), nearly 100% of the discharge power would have to be channeled into thermal energy of the neutrals—an unlikely scenario. We believe therefore, that the difference must be due in part to the existence of a slip condition under these low pressure environments. As discussed in Sec. III, a temperature slip can account for nearly 90 K of the 200 K temperature difference. Conditions where $\beta \sim 0.5$ can easily account for the rest. Finally, this analysis supports our assumption of the use of the original model of Davis and Vanderslice [6] in the interpretation of our results in that any temperature variation for reasonable values of β are certainly within the uncertainty in the measurements of the temperature in our experiments.

[1] A. von Engel, *Ionized Gases* (Oxford University Press, Oxford, 1955), p. 255.
[2] G. Francis, *Handbuch der Physic*, edited by S. Flugge (Springer, Berlin, 1956), Vol. 22, p. 70.
[3] S.-J. Park, C. J. Wagner, C. M. Herring, and J. G. Eden, Appl. Phys. Lett. **77**, 199 (2000).
[4] R. M. Sankaran and K. P. Giapis, Appl. Phys. Lett. **79**, 593 (2001).
[5] T. Ito, N. Gascon, W. S. Crawford, and M. A. Cappelli, Proceedings of the 29th International Electric Propulsion Conference, Princeton, NJ, October 31–November 4, IEPC-2005–198 (2005).
[6] W. D. Davis and T. A. Vanderslice, Phys. Rev. **131**, 219 (1963).
[7] S. B. Radovanov, R. J. Van Brunt, J. K. Olthoff, and B. M. Jelenkovic, Phys. Rev. E **51**, 6036 (1995).
[8] M. V. V. S. Rao, R. J. Van Brunt, and J. K. Olthoff, Phys. Rev. E **54**, 5641 (1996).
[9] C. V. Budtz-Jørgensen, J. Bøttiger, and P. Kringhøj, Vacuum **56**, 9 (2003).
[10] C. V. Jurgensen, J. Appl. Phys. **64**, 590 (1988).
[11] I. Abril, A. Gras-Marti, and J. A. Vallés-Abarca, Phys. Rev. A **28**, R3677 (1983).
[12] V. V. Serikov and K. Nanbu, J. Appl. Phys. **82**, 5948 (1997).
[13] I. Revel, L. C. Pitchford, and J. P. Boeuf, J. Appl. Phys. **88**, 2234 (2000).
[14] G. Gamez, A. Bogaerts, G. Andrade, and G. M. Hieftje, Spectrochim. Acta, Part B **59**, 435 (2004).
[15] A. Bogaerts, R. Gijbels, G. Gamez, and G. M. Hieftje, Spectrochim. Acta, Part B **59**, 449 (2004).
[16] P. S. Kothnur, X. Yuan, and L. L. Raja, Appl. Phys. Lett. **82**, 529 (2003).
[17] C. Penache, M. Miclea, A. B.-Demian, O. Hohn, S. Schössler, T. Jahnke, K. Niemax, and H. S.-Böcking, Plasma Sources Sci. Technol. **11**, 476 (2002).
[18] F. Leipold, R. H. Stark, A. El-Habachi, and K. H. Schoenbach, J. Phys. D **33**, 2268 (2000).
[19] A. V. Phelps, Plasma Sources Sci. Technol. **10**, 329 (2001).
[20] A. V. Phelps, J. Phys. Chem. Ref. Data **20**, 557 (1991).
[21] D. P. Aeschliman, R. A. Hill, and D. L. Evans, Phys. Rev. A **14**, 1421 (1976).
[22] K. Tachibana, H. Hirano, and Y. Urano, J. Phys. B **15**, 3169 (1982).
[23] O. Leroy, J. Perrin, J. Jolly, M. Péalet, and M. Lefebvre, J. Phys. D **30**, 499 (1997).
[24] J. M. Candhi and S. C. Saxena, J. Chem. Eng. Data **13**, 357 (1968).
[25] A. J. Rothman and L. A. Bromley, Ind. Eng. Chem. **47**, 899 (1955).
[26] *NIST-JANAF Thermochemical Tables*, edited by M. W. Chase, Jr. (American Institute of Physics for the National Institute of Standards and Technology, New York, 1998).
[27] M. A. Lieberman and A. J. Lichtenberg, *Principles of Plasma Discharges and Materials Processing* (Wiley, New York, 1994), p. 170.